Journal of Techniques, ISSN: 2708-8383, Vol. 7, No. 4, 2025, Pages 103-115
DOI: https://doi.org/10.51173/jt.v7i4.2713

JOURNAL OF TECHNIQUES

Journal homepage: http://journal.mtu.edu.iq

RESEARCH ARTICLE - MATERIALS SCIENCE (MISCELLANEOUS)

A Novel Approach to Electrophoretic Deposition of Bioactive Glass on Ti-6Al-7Nb Using TEA-Stabilized Suspension

Anmar Tallal Kadhim[1*], Ayad Naseef Jasim[1], Alaa A. Atiyah[2], Hanaa Soliman[3], Sumair Ahmed Soomro[4]

[1]College of Engineering, University of Diyala, Baquba, Iraq

[2]University of Technology, Baghdad, Iraq

[3]Central Metallurgical Research and Development Institute (CMRDI), Helwan, Egypt

[4]Key Laboratory of Advanced Technologies of Materials, Ministry of Education, School of Materials Science and Engineering, Southwest Jiaotong University, Chengdu 610031, China

[*] Corresponding author E-mail: materials_grad_23_6@uodiyala.edu.iq

Article Info.

Article history:

Received
08 July 2025

Revised
06 August 2025

Accepted
15 August 2025

Published
31 December 2025

Abstract

This study investigated the effect of varying bioactive glass (BG) concentrations (8–14 g/L) on the structural, electrochemical, and adhesive properties of coatings deposited on Ti-6Al-7Nb substrates via electrophoretic deposition (EPD). The SEM and EDS analyses demonstrated that rising BG concentration from 8 g/L to 14 g/L enhanced the coating uniformity, reduced the porosity and enhanced the particle packing. The coating thickness increased from 41.1 µm to 57.3 µm. Zeta potential measurements showed increased suspension stability with higher BG content, reaching 18.47 mV at 14 g/L. Corrosion resistance is enhanced with BG content, with the 14 g/L coating reaching the lowest corrosion current density (5.19×10^{-8} A) and rate (4.509×10^{-4} mmpy). Adhesion tests rated the 14 g/L BG coating as 1B due to better interlocking.

Publisher: Middle Technical University

Keywords: Bioactive Glass; Triethanolamine; Electrophoretic Deposition Ti-6Al-7Nb Alloy; Zeta Potential; Corrosion Resistance; Adhesion Strength.

1. Introduction

The world population continues to rise and people are living longer lives, resulting in increased demand for adequate skeletal repair options [1-3]. Metallic implants are used to replace missing or damaged hard tissues because they can give mechanical strength to load-bearing functions. Titanium alloys, stainless steels and iron alloys, cobalt-chromium alloys, and tantalum are the most common metals used for making implants. All metals used in implants have the good property of good biocompatibility; the human body typically does not generate adverse reactions upon implantation [4- 6].

Although these metals possess excellent mechanical support, they are typically bioinert (can provide mechanical support without excessive interaction in the biological environment). Consequently, surface modification (usually in the form of a bioactive coating) can enhance biological camaraderie. These coatings can stimulate chemical interaction and/or cellular activity at the implant site, resulting in the formation of a stable and strong bond with surrounding bone tissue. These added bioactive layers improved long-term performance of the implant and minimized revision surgeries because of improved osseointegration/stability [7- 14].

Bioactive glasses demonstrate high reactivity in physiological conditions, making them suitable candidates for hard tissue repair [15, 16]. Bioactive glasses demonstrate high reactivity in physiological conditions, making them suitable candidates for hard tissue repair [17]. Over the past fifty years, researchers have expanded their scope to include other glass chemistries, showing that bioactive glasses can be used as coatings in biomedical devices [18-20]. The use of bioactive glass as a coating on metallic implants has grown significantly, based on its ability to interact with body fluids and stimulate bone bonding and integration [21, 22].

Nomenclature & Symbols			
Ti-6Al-7Nb	Titanium alloy with 6% Aluminum and 7% Niobium	SEM	Scanning Electron Microscope
ZP	Zeta Potential	EDS	The Energy Dispersive Spectroscopy
HA	Hydroxyapatite	XRD	X-ray Diffraction
CS	Chitosan	µm	Micrometer
EPD	Electrophoretic Deposition	mV	Millivolt
Sq	Root Mean Square Roughness	MPa	Megapascal
Sa	Arithmetic Mean Roughness	mm/year	Millimeters per Year
ASTM	American Society for Testing and Materials	Ω·cm²	Ohm Square Centimeters
SBF	Simulated Body Fluid	g/L	Grams per Liter
FTIR	Fourier Transform Infrared Spectroscopy	V	Volt

These coatings are often considered a valuable alternative to calcium phosphate Bioactive glass coatings can be considered a preferable alternative to calcium phosphate coatings due to their superior bioactivity in physiological conditions. Many types of bioactive glasses of various chemistries have been studied for bioactivity, understanding bioactivity is now an emerging focus of studies for surface coatings for metallic bone implants [18, 23, 24]. Bioactive glass coatings have shown considerable promise as better alternatives to conventional calcium phosphate coatings as they have high chemical reactivity in physiological environments [25, 26]. Here are many procedures that can be used to apply bioactive glass to implant surfaces, such as plasma-spraying, laser cladding, magnetron sputtering, sol–gel techniques, dip- or spin-coating, and EPD (electrophoretic deposition). In recent years, EPD has attracted particular interest from both the academic and industrial sectors as it enables the production of uniform, well-adhered coatings at low post-processing temperatures and also commercially inexpensive and simplistic equipment [23, 25, 27-30]. The deposition process can be carried out using a stable colloidal suspension by selecting positively or negatively charged bioactive glass particles, and applying an electric field, In dry EPD, the bioactive-glass suspension particles carry some kind of surface charge, and once EPD is applied, the charged particles are directed toward the substrate under the electric field, and form a consistent coating layer via EPD [31- 38].

This research provides a systematic optimization of the electrophoretic deposition (EPD) parameters (voltage, time and bioactive glass (BG) concentration) for coating the Ti-6Al-7Nb substrates using a TEA-stabilized isopropanol-based suspension. This study is the first to use triethanolamine (TEA) as a dispersion agent, which is hypothesized to improve the BG particle size uniformity within the coating suspension, leading to an improved homogeneity of the coating. This study incorporates the controlled EPD conditions, and a thorough evaluation of the deposition after the EPD process, to achieve high-quality, crack-free BG coatings with a strong adhesion — all of which are optimized for biomedical uses.

2. Experimental Work

2.1. Materials

The bioactive glass material that was used and analyzed in this study was supplied by Qingdao Spring Glass Company Limited (China). The nominal chemical composition can be determined to be 45 wt% SiO_2, 24.5 wt% CaO, 24.5 wt% Na_2O and 6 wt% P_2O_5; this corresponds to the generally accepted chemical formulation of 45S5 Bioglass. Chitosan that was used for this study was supplied by Jinan Refine Chemical Co., Ltd. (China), and it has a degree of acetylation from 80% to 95%. The chitosan was used in the suspension at a concentration of 0.5 g/L (as a natural polymeric binder) for the purposes of assisting with particle adhesion during the electrophoretic deposition process. Ethanol (Alpha Chemika, India) was the solvent used for the dissolution of chitosan and to achieve a stable, uniform suspension. Organic compound Triethanolamine (TEA) was supplied by Shiguang (Hebei) Supply Chain Management Co., Ltd.

2.2. Preparation and electrophoretic deposition of bioactive glass and triethanolamine coating

A coating solution was prepared by mixing isopropanol, followed by the addition of triethanolamine (TEA) (25 mL in total). TEA was used to stabilize the suspension and enhance the dispersion of bioactive glass (BG) particles within the solvent. The components were stirred using a magnetic stirrer for 10 minutes to ensure proper mixing. BG was then added to the solution in various concentrations (as shown in Table 1), and the total mixture volume was adjusted to 25 mL using isopropanol. The solution underwent 2 hours of continuous mixing with a magnetic stirrer before receiving 30 minutes of ultrasonic treatment to reach complete homogenization. After preparation, the coating process was carried out on samples using the EPD method under various experimental conditions, with voltages of 20, 40, and 60 V, times of 2, 4, and 6 minutes, and BG concentrations of 8, 11, and 14 g/L, as shown in Table 1.

After systematic testing, the optimal coating conditions were identified and are presented in Table 2 and Fig. 1 show the electrophoretic deposition process for coating Ti-6Al-7Nb substrates with bioactive glass.

Table 1. Bioactive glass and triethanolamine coating conditions

Sample No.	Voltage (V)	Time (min)	BG concentration (g/L)
1	20	2	8
2	20	4	11
3	20	6	14
4	40	2	11
5	40	4	14
6	40	6	8
7	60	2	14
8	60	4	8
9	60	6	11

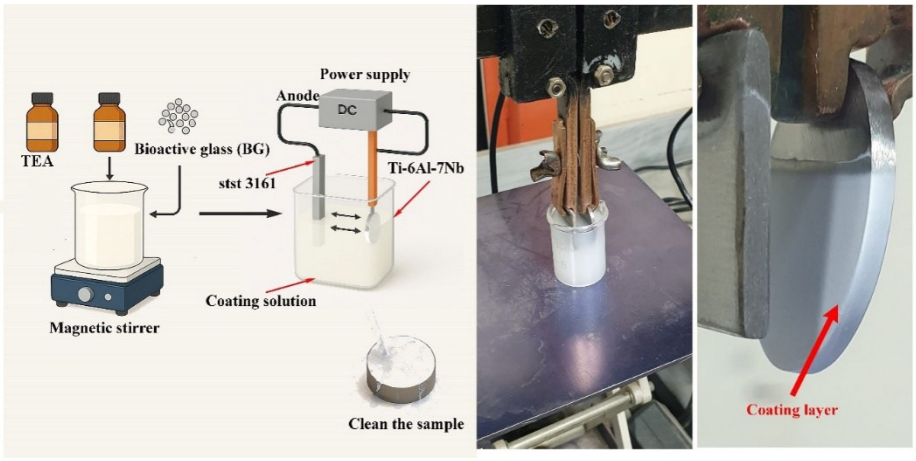

Fig. 1. The electrophoretic deposition (EPD) process for coating Ti-6Al-7Nb substrates with bioactive glass (BG)

Table 2. Optimal EPD coating parameters using BG concentrations at constant time and voltage

Sample No.	Time (min)	Voltage (V)	BG concentration (g/L)
1	6	60	8
2	6	60	11
3	6	60	14

2.3. Characterization and testing

The corrosion behavior of Ti6Al7Nb alloy samples was studied using a potentiostat (CHI 604E, China) in a simulated body fluid (SBF) solution. The SBF solution composition is shown in Table 3, and all the chemicals used were of analytical grade from CDH, India. The electrochemical tests included open circuit potential (OCP) and potentiodynamic polarization (Tafel) to assess the corrosion resistance of the samples. The best corrosion resistance was observed in one of the samples, which was selected for further analysis. This sample was placed in SBF at 37 °C for one month to mimic the long-term exposure to physiological conditions. After immersion, the sample was heat-treated at 400 °C for one hour to study the effect of thermal treatment on its surface features and corrosion behavior.

The cross-cut tape test based on ASTM D3359 standard was used to evaluate the coating adhesion strength. The test evaluates substrate-coating adhesion through a procedure that involves cutting a grid pattern in the coating before applying and removing pressure-sensitive adhesive tape. The visual examination of the area after tape removal determines the degree of coating detachment. The adhesion rating ranges from 0B to 5B where 5B shows no removal for excellent adhesion and 0B shows more than 65% coating removal for poor adhesion. The test offers a fast and effective method to evaluate the integrity of coating-substrate interfaces under controlled testing conditions [39]. The Inspect F 50 FEISEM (Eindhoven, The Netherlands) was used to study the surface morphology and coating thickness of Ti-6Al-7Nb and Ti alloy samples. The X-ray diffraction (XRD) system (Plate Number 1, NF type) with Cu target (Kα = 1.54 Å), Model XRD-6000, and X-ray tube of the same type was used to identify the phases present in the coating layer.

The antibacterial testing utilized the agar well diffusion method. The bacterial strains used for testing included Escherichia coli (Gram-negative) and Staphylococcus aureus (Gram-positive) purchased from a certified microbiology laboratory culture collection. Non-frozen bacterial suspensions were prepared from nutrient broth to obtain a 0.5 McFarland standard before inoculating nutrient agar. Coated samples were inoculated in wells and incubated at 37 °C for 24 hours. Inhibition zones around the samples were measured in millimeters.

Table 3. Chemical composition of simulated body fluid (SBF) solution [40]

ITEM	Reagent	Concentration g/l
1	8.035	NaCl
2	0.355	$NaHCO_3$
3	0.225	KCl
4	0.231	K_2HPO_4
5	0.311	$MgCl_2.6H_2O$
6	0.292	$CaCl_2$
7	0.072	Na_2SO_4

3. Results and Discussion

3.1. Surface morphology of BG-coated Ti-6Al-7Nb substrates via EPD under varying BG concentrations

The SEM analysis of Ti-6Al-7Nb substrates with different bioactive glass (BG) concentrations through electrophoretic deposition (EPD) appears in Fig. 2. The uncoated sample Fig. 2a displays a smooth surface with visible polishing marks and no particle deposition which confirms the bare metal condition. The surface of 8 g/L BG concentration Fig. 2b shows porosity and irregular particle distribution and incomplete coverage according to both low and high magnification images. The surface becomes more uniform and denser when the BG concentration reaches 11 g/L Fig. 2c while the particle packing improves and voids decrease. The surface at 14 g/L Fig. 2d displays the most compact and continuous coating structure because it contains densely packed particles with minimal porosity and well-integrated structures. The highest BG concentration of 14 g/L produces the most effective coating conditions, which result in uniform and adherent layers on Ti-6Al-7Nb substrates.

3.2. Cross-sectional SEM analysis of BG coating thickness at different concentrations

The SEM images in Fig. 3 display Ti-6Al-7Nb substrates that received different bioactive glass (BG) concentrations through the EPD method. The measurements of coating thickness served to determine how different BG concentrations affect the deposited layer. The 8 g/L Fig. 3a sample shows a 41.1 µm-thick coating that appears thin and loosely packed. The BG concentration increase to 11 g/L Fig. 3b produces a 56.8 µm thick coating with dense and continuous particle accumulation. The 14 g/L BG sample Fig. 3c demonstrates the thickest and most compact coating which reaches 57.3 µm. The experimental results show that higher BG concentrations produce thicker coatings because they provide better particle availability and improved deposition efficiency. The observed increase in thickness matches the Zeta Potential findings regarding enhanced zeta potential and surface coverage.

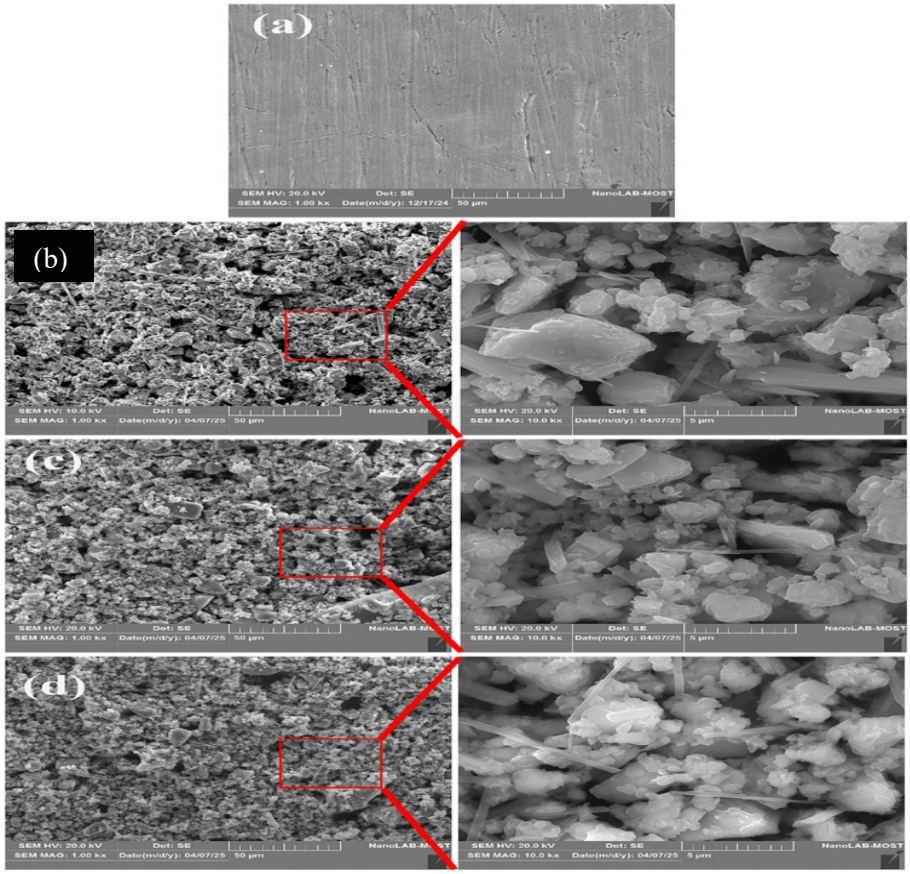

Fig. 2. SEM images of Ti-6Al-7Nb substrates coated with bioactive glass (BG) using the electrophoretic deposition (EPD) method at different BG concentrations: (a) uncoated substrate, (b) coated with 8 g/L BG, (c) coated with 11 g/L BG, (d) coated with 14 g/L BG

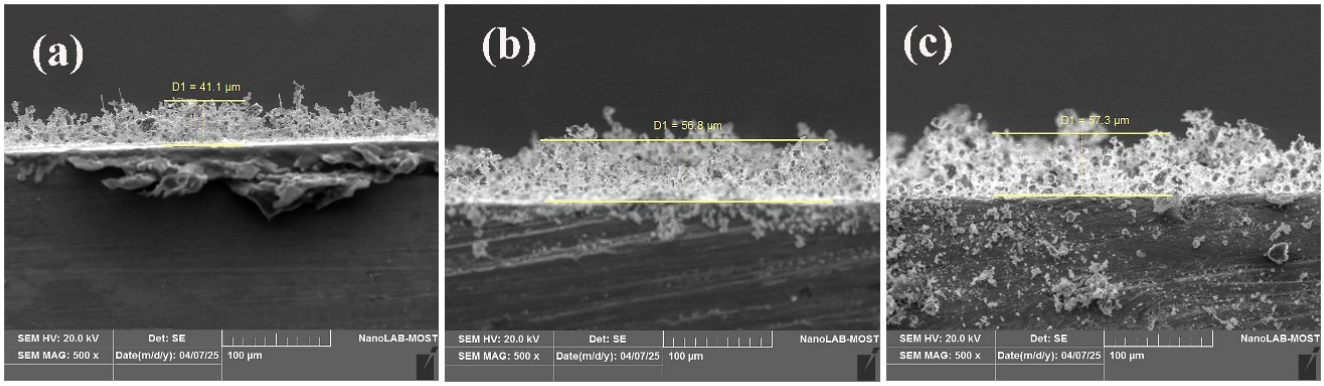

Fig. 3. Cross-sectional SEM images showing the coating thickness of BG layers deposited on Ti-6Al-7Nb substrates at different BG concentrations using the EPD method: (a) 8 g/L, (b) 11 g/L, (c) 14 g/L

3.3. Elemental composition analysis of BG-coated Ti-6Al-7Nb samples at varying BG concentration

Fig. 4 presents the energy-dispersive X-ray spectroscopy (EDS) results of Ti-6Al-7Nb substrates coated with three different concentrations of bioactive glass (BG) using the electrophoretic deposition (EPD) method. All spectra confirm the successful deposition of BG through the presence of oxygen (O), sodium (Na), silicon (Si), phosphorus (P), and calcium (Ca) in varying weight percentages. As the BG concentration

increases from 8 g/L (Fig. 4a) to 14 g/L (Fig. 3c), the intensity of BG-related elements (especially Si and Ca) slightly increases, while the detected titanium (Ti) signal from the substrate decreases. This suggests improved surface coverage and thicker BG coating at higher concentrations. The (Ti) content shows a major reduction from 6.49 wt% at 8 g/L to 1.55 wt% at 14 g/L which indicates better substrate coverage. The Si content rises from 15.95 wt% to 17.25 wt% and the Ca content rises from 13.61 wt% to 16.01 wt% because of increased BG deposition. The SEM images on the right side of each spectrum show that the surface coverage and morphology remain consistent throughout all concentration levels.

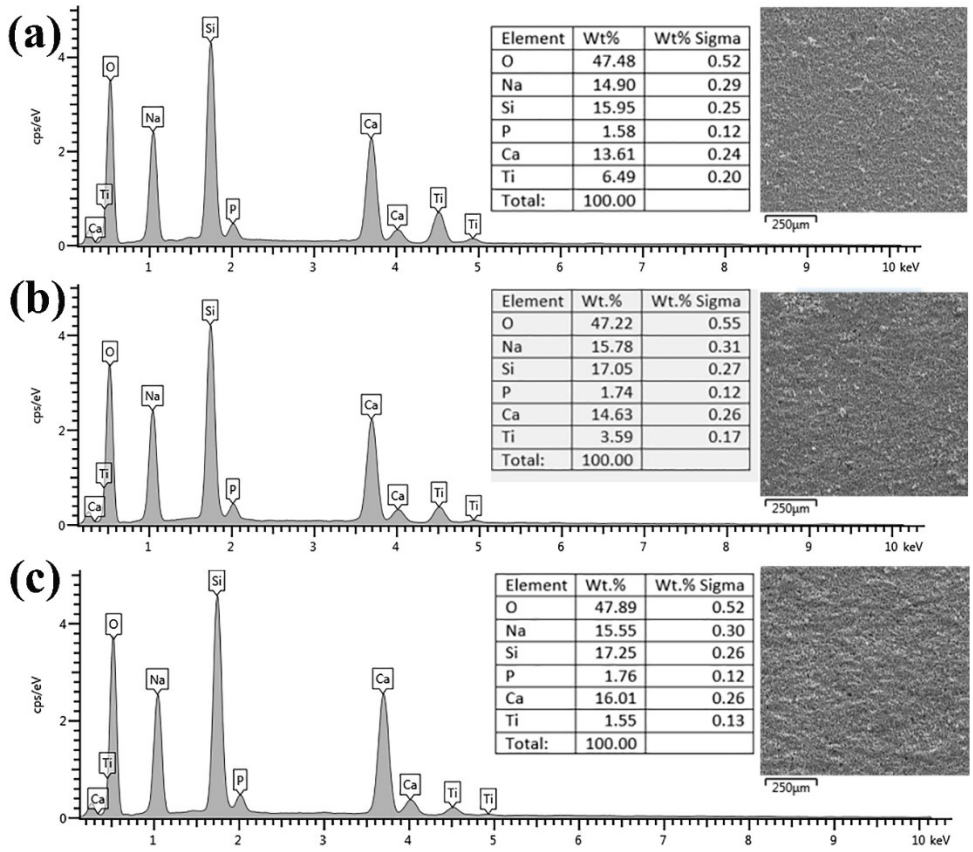

Fig. 4. EDS spectra, elemental composition (Wt.%), and SEM images of Ti-6Al-7Nb substrates coated with different concentrations of bioactive glass (BG) using the EPD method: (a) 8 g/L, (b) 11 g/L, (c) 14 g/L

3.4. Zeta potential measurement of BG suspensions at different concentrations

The zeta potential measurements of bioactive glass (BG) suspensions at different concentrations (8, 11, and 14 g/L) appear in Fig. 5. The zeta potential serves as a critical indicator for colloidal suspension stability because higher values indicate better dispersion and reduced particle agglomeration. The zeta potential measurements at 8 g/L and 11 g/L show similar values of 11.84 mV and 11.97 mV which indicate moderate suspension stability. The zeta potential reaches 18.47 mV when the BG concentration reaches 14 g/L. The increased repulsive forces between particles lead to better suspension stability. The increased zeta potential at higher concentrations leads to improved particle distribution uniformity which enhances EPD process coating quality [41, 42].

3.5. Adhesion performance of BG coatings evaluated by cross-cut tape test

Fig. 6 and Table 4 show the adhesion behavior of BG coatings on Ti-6Al-7Nb substrates using the cross-cut tape test, according to ASTM D3359 standards. The visual observations in Fig. 6(a, b, and c) correspond to BG concentrations of 8, 11, and 14 g/L, respectively. The 8 g/L BG Fig. 6a sample demonstrated average adhesion strength because 20% of the coating material detached during testing which placed it in the 2B classification. The 11 g/L sample Fig. 6b showed slightly lower adhesion with 25% area removal, also rated as 2B. The 14 g/L BG-coated sample Fig. 6c displayed outstanding adhesion properties because it lost only 3% of its coating material which received a 1B classification. The improved adhesion at elevated BG concentrations results from better coating uniformity and surface coverage and a more compact coating structure which SEM and EDS results demonstrate [43]. The research shows that higher BG concentrations simultaneously enhance both surface thickness and morphology and create stronger substrate-coating bonds [44].

Table 4. Adhesion test results of BG-coated Ti-6Al-7Nb substrate at different BG concentrations using the cross-cut tape method

Sample	Percent area removed (%)	Classification
8 gm/l	20	2B
11 gm/l	25	2B
14 gm/l	3	1B

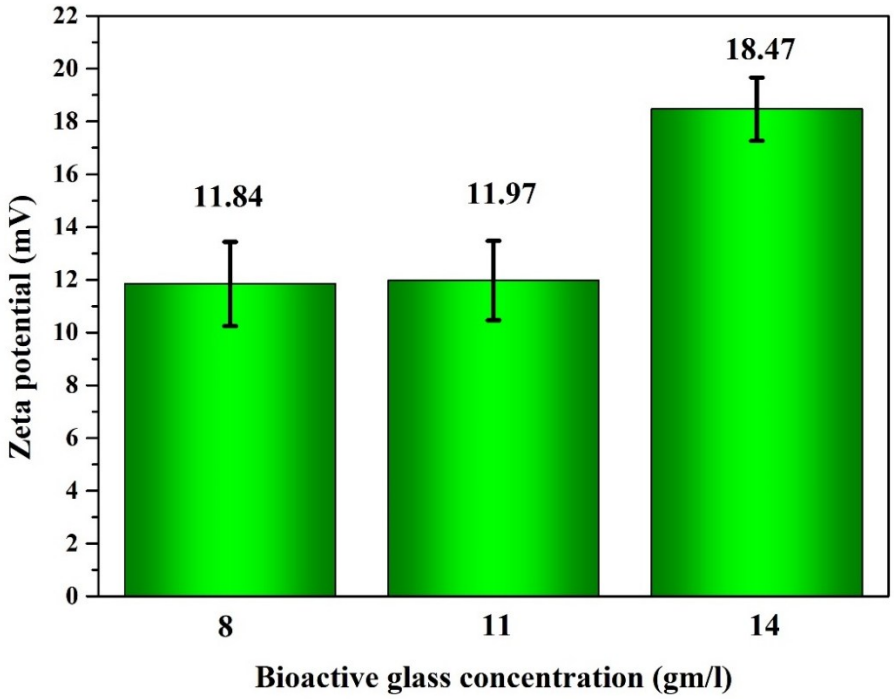

Fig. 5. Zeta potential values of bioactive glass (BG) suspensions at concentrations of 8, 11, and 14 g/L

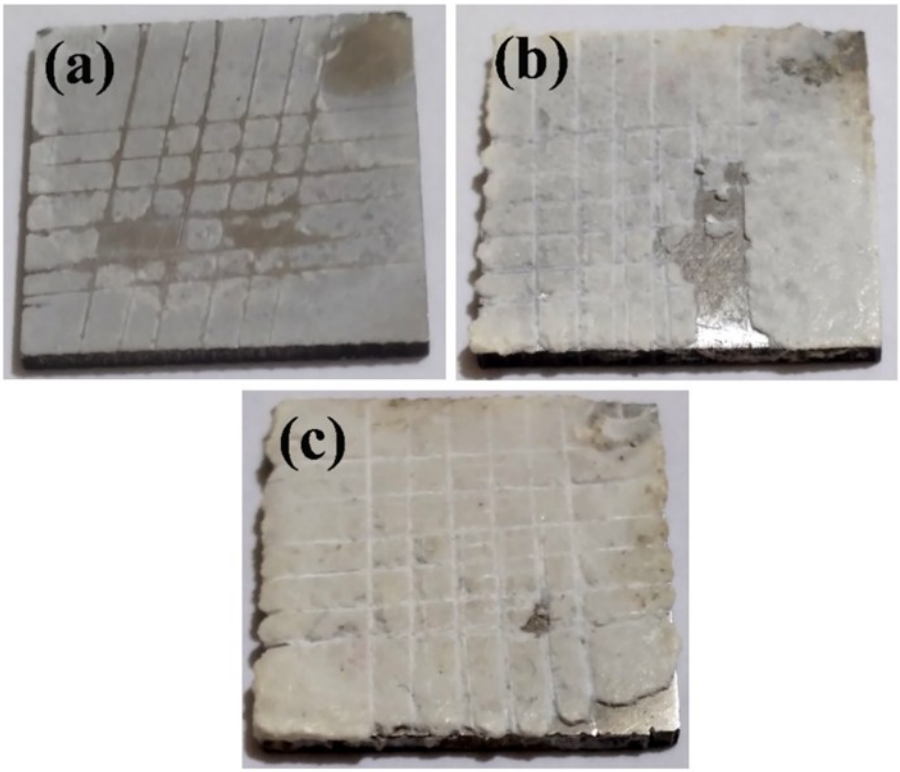

Fig. 6. Cross-cut tape adhesion test for Ti-6Al-7Nb substrates coated with bioactive glass (BG) at different concentrations: (a) 8 g/L, (b) 11 g/L, (c) 14 g/L

3.6. Electrochemical corrosion performance of BG-coated Ti-6Al-7Nb in simulated body fluid

The electrochemical behavior of Ti-6Al-7Nb samples with different bioactive glass concentrations is shown in Fig. 7 and Table 5, through Tafel polarization curves and extracted corrosion parameters. The uncoated base sample shows high corrosion current density and negative potential shift indicating poor corrosion resistance. The addition of 8 g/L BG results in a moderate decrease of corrosion current to 3.154×10^{-7} A and corrosion rate to 2.740×10^{-3} mmpy. The corrosion resistance improves with 11 g/L BG coating which results in a corrosion current of 1.151×10^{-7} A and a corrosion rate of 1.000×10^{-3} mmpy. The highest performance is achieved with 14 g/L BG which shows the lowest corrosion

current of 5.190 × 10^{-8} A and the lowest corrosion rate of 4.509 × 10^{-4} mmpy. The open circuit potential (OCP) becomes more positive as the BG content increases which indicates better surface passivation. The electrochemical stability of the coating improves with increasing BG concentration, and 14 g/L shows the best corrosion barrier performance.

Table 5. Electrochemical corrosion parameters of BG-coated Ti-6Al-7Nb samples at different BG concentrations in SBF

ITEM	E corr. (volt)	I corr. (Amp.)	Corr. Rate (mmpy)	βC	βa	OCP (volt)
8 gm/l	-0.446	3.154× 10^{-7}	2.740 × 10^{-3}	0.197	0.208	-0.420
11 gm/l	-0.136	1.151× 10^{-7}	1.000 × 10^{-3}	0.196	0.211	-0.233
14 gm/l	-0.211	5.190 × 10^{-8}	4.509 × 10^{-4}	2.127	0.180	-0.156

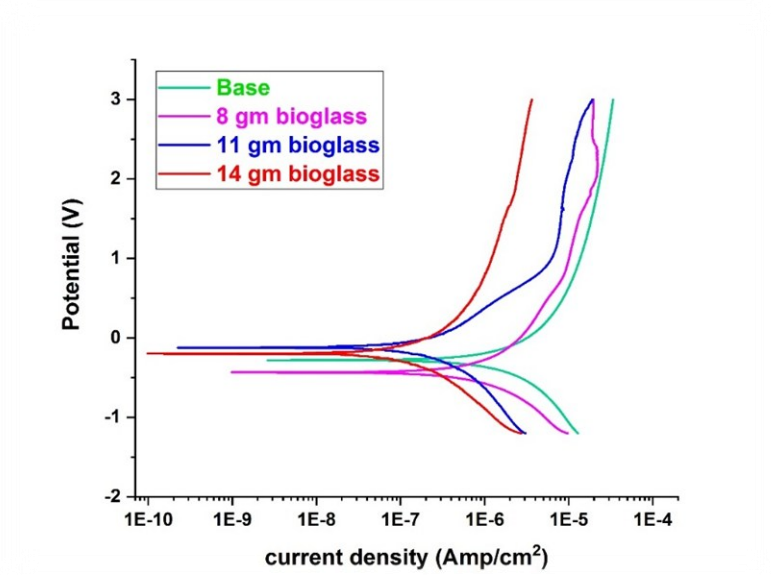

Fig. **7**. Tafel polarization curves of Ti-6Al-7Nb samples coated with different concentrations of bioactive glass (BG) in simulated body fluid (SBF)

3.7. Antibacterial performance of BG-coated Ti-6Al-7Nb substrates

The antibacterial activity of Ti-6Al-7Nb substrates coated with bioactive glass (BG) dispersed in isopropanol was evaluated using the well agar diffusion method. The coated samples demonstrated clear inhibition zones against both *Escherichia coli* and *Staphylococcus aureus*. The inhibition zone against *E. coli* reached 26 mm, while the zone against *S. aureus* was 23 mm, as shown in Fig. 8 (a and b). These results confirm the antibacterial potential of BG coatings, particularly due to ionic dissolution products (e.g., Ca^{2+}, Na^{+}, Si^{4+}) that disrupt bacterial membranes. Compared to the uncoated Ti-6Al-7Nb samples, which exhibited larger zones (42 mm for *E. coli* and 37 mm for *S. aureus*), the coated surfaces still maintained considerable antimicrobial effectiveness, offering a balance between bioactivity and surface protection. While the coated samples showed antibacterial activity, the uncoated Ti-6Al-7Nb alloy exhibited slightly larger inhibition zones in some cases. This was surprising because of the potentially positive effects from the release of metallic ions (for example, Al or Nb) from the bare alloy surface, which can have slightly moderate antibacterial effects by disrupting bacterial membranes and metabolic processes. The properties of the coating should serve as a physical barrier to prevent the release of ions from the substrate. Similarly, the coated surfaces required a dissolution/hydrolysis process (release of ions) to initiate antibacterial activity, which may have influenced the size of the inhibition zone to be smaller or not as immediate as the bare alloy. For the coated samples, after longer exposure periods, the release of ions could help maintain antibacterial performance due to continued ion release and growth of the apatite layer.

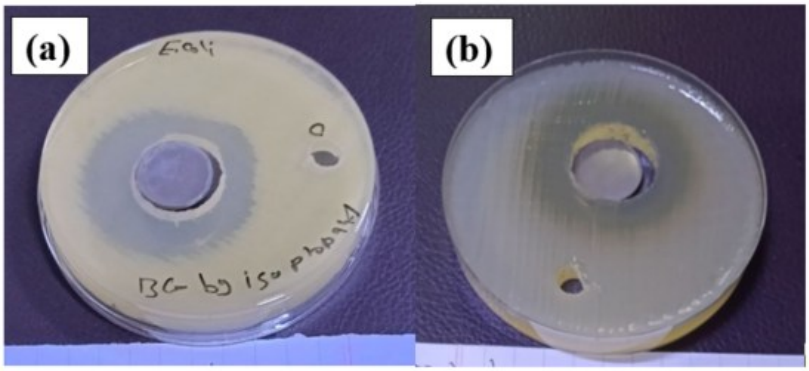

Fig. 8. Photographs of BG-coated Ti-6Al-7Nb samples using isopropanol suspension tested for antibacterial activity by the well agar diffusion method:(a) inhibition zone of 26 mm against Escherichia coli, (b) inhibition zone of 23 mm against Staphylococcus aureus

3.8. Effect of Bioglass concentration on wettability of EPD-coated surfaces

The contact angle measurements for coatings made from different bioactive glass concentrations (8, 11, and 14 g/L) appear in Table 6 and Fig. 9. The contact angle measurements show an upward trend with increasing bioglass concentration starting from 10.983° at 8 g/L and reaching 14.133° at 11 g/L before ending at 21.185° at 14 g/L. The surface becomes less water-attractive because higher BG concentrations create roughness and particle clumps and reveal more silicate elements. The research indicates that lower BG concentrations produce better wettability which could lead to superior biointegration performance [45].

Table 6. Contact angle values (in degrees) of EPD-coated Ti-6Al-7Nb samples prepared with different bioglass concentrations. The data reflect the effect of BG content on surface wettability

Sample	Contact angel (degree)
8 gm/l	10.983
11 gm/l	14.133
14 gm/l	21.185

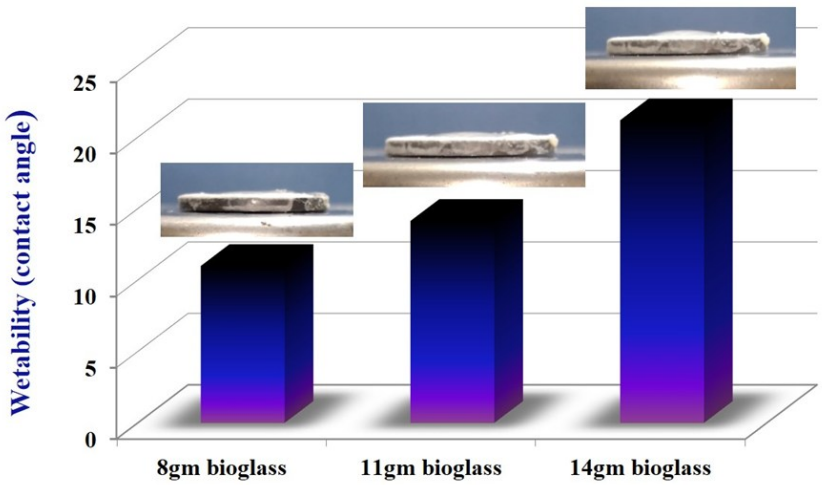

Fig. 9. Contact angle values of coatings deposited with different bioglass concentrations (8, 11, and 14 g/L)

3.9. Elemental mapping of coated surface after immersion in simulated body fluid (SBF)

The elemental distribution maps in Fig. 10 reveal the surface composition of the coated Ti-6Al-7Nb sample after it was submerged in simulated body fluid (SBF). The metal surface shows a Ca-P-rich layer because O (49.6 %), Ca (11.5%), Na (14.5 %), and P (4.6%) are the most abundant elements. The presence of magnesium (2.8 %), silicon (1.6 %), and potassium (1.2 %) supports the contribution of the original bioactive glass (BG) composition. The SBF solution contains Na, K, Mg, Ca, P, and O elements, which come from the solution that mimics human plasma ion composition. Their presence confirms the ion exchange between the BG-coated surface and the surrounding fluid, promoting surface reactivity and biomineralization. The increase in Ca and P especially indicates apatite nucleation, a key marker of bioactivity. The uniform elemental distribution further implies good coating stability and strong interaction with the physiological environment.

3.10. Surface structure of BG-coated Ti-6Al-7Nb after SBF immersion

The SEM micrographs in Fig. 11 show the surface morphology of the Ti-6Al-7Nb alloy coated with 14 g/L bioactive glass (BG) after 30 days of immersion in simulated body fluid (SBF). The low-magnification image (left) shows a dense and continuous layer covering the entire surface, indicating effective deposition and post-immersion surface transformation. The high-magnification image (right) shows a fine, granular structure made of nanoscale spherical particles. These features confirm the formation and growth of an apatite-like layer. The observed morphology indicates successful ion exchange between the BG-coated surface and the SBF, resulting in the nucleation and accumulation of calcium and phosphate ions from the solution. The uniform and compact structure suggests stable bioactivity and high surface reactivity. The fine particles represent apatite crystallites that formed as a result of the gradual release of Na^{+}, Ca^{2+}, and Si^{4+} ions from the bioactive glass, which triggered the biomimetic mineralization [46].

3.11. Elemental composition analysis of BG (14 g/L)-coated Ti-6Al-7Nb surface after SBF immersion

The EDX spectra in Fig. 12 and Table 7 verify the elemental composition of the BG (14 g/L)-coated Ti-6Al-7Nb surface after one month of immersion in simulated body fluid (SBF). The detected elements include oxygen (O), sodium (Na), magnesium (Mg), aluminum (Al), silicon (Si), phosphorus (P), chlorine (Cl), potassium (K), and calcium (Ca). The presence of high-intensity peaks for Ca and P suggests the formation of a calcium-phosphate-rich layer, confirming that an apatite had been grown onto the surface. Silicon and sodium were also present on the surface, indicating that the contributions from the bioactive glass also aided in surface bioactivity. Cl, K, and Mg indicated these ions were exchanged with the SBF solution which contains ions associated with simulated plasma. This supports that the surface had interacted with the environment to incorporate ions and reprecipitate in vivo. The presence of two distinct Ca peaks and a high intensity peak for Cl indicates a higher mineralization and activation of the surface. The consistent, well-defined elemental signals indicate a homogenous substrate coating, which has maintained a stable interface over a long period of time, and confirms the SEM evaluation of a densely compact layer consisting of small nanoparticles. Collectively, these results indicate the bioactive and chemically stable nature of the BG-coated surface.

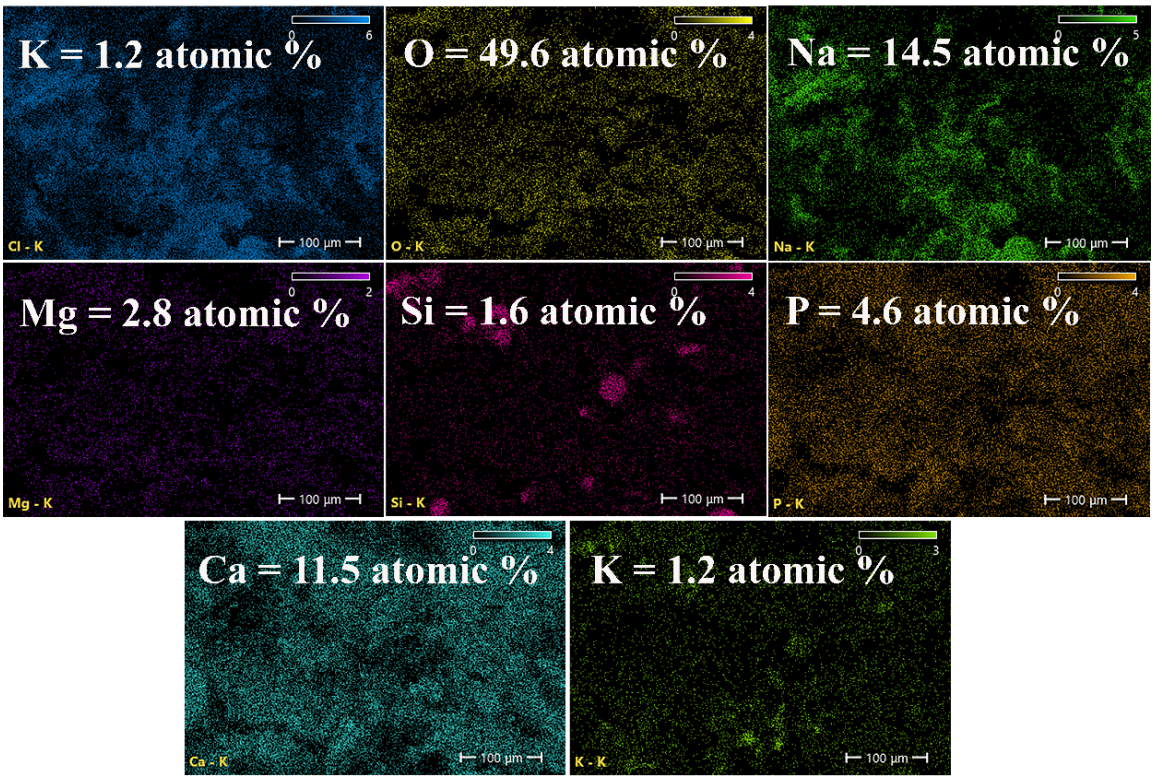

Fig. 10. EDS elemental mapping of the coated Ti-6Al-7Nb surface after immersion in simulated body fluid (SBF)

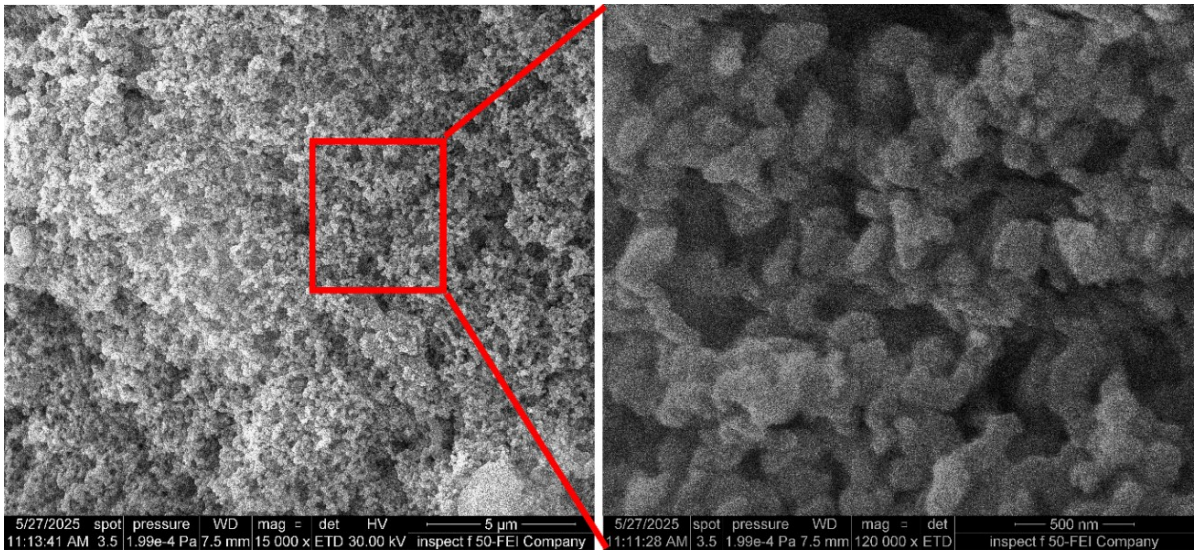

Fig. 11. SEM images of the BG-coated Ti-6Al-7Nb substrate after immersion in simulated body fluid (SBF)

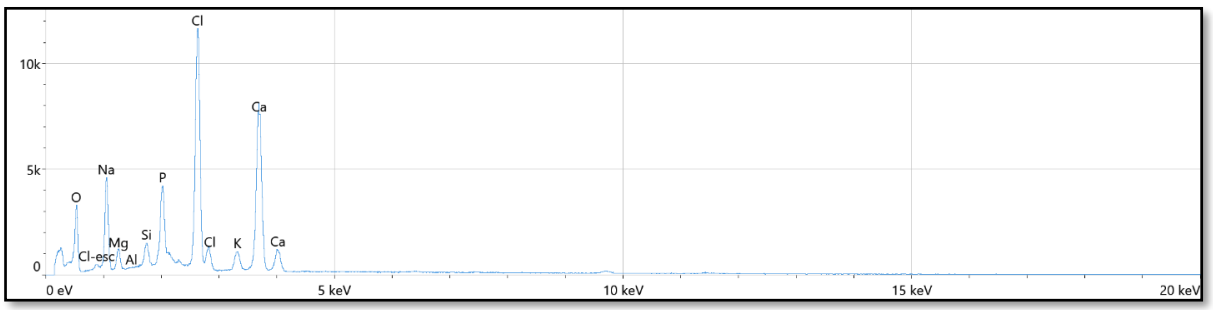

Fig. 12. EDX spectra of Ti-6Al-7Nb substrate coated with 14 g/L bioactive glass (BG) after one month of immersion in simulated body fluid (SBF)

Table 7. Elemental analysis of the BG-coated Ti-6Al-7Nb surface after immersion in simulated body fluid (SBF) as identified by EDX spectroscopy

Element	Atomic %
O	49.6
Na	14.5
Mg	2.8
Al	0.0
Si	1.6
P	4.7
Cl	14.2
K	1.2
Ca	11.5

3.12. Electrochemical performance of BG-coated Ti-6Al-7Nb after SBF immersion

Electrochemical analysis of the 14 g/L BG-coated Ti-6Al-7Nb substrate after SBF immersion demonstrates a significant improvement in corrosion protection. As noted above with the OCP curve Fig. 13a and Table 8, the increase from –0.156 V to –0.011 V following immersion indicates improved passivation performance. The Tafel polarization results Fig. 13b show a downward shift of corrosion current density (I_{corr}) from 5.190×10^{-8} A to 2.387×10^{-8} A and a reduction of the corrosion rate from 4.509×10^{-4} to 2.073×10^{-4} mmpy. The electrochemical analysis of the 14 g/L BG-coated Ti-6Al-7Nb substrate after SBF immersion shows a significant ~54% decrease further supporting that immersion in SBF allows for apatite growth and surface sealing.

There was a beta value increase from 0.180 to 0.213 which suggests improved anodic passivation, with the beta value conditionally invariant at 0.197 ensuring that cathodic activity is suppressed. The improved electrochemical behaviour is attributed to the formation of a dense bioactive apatite layer that improved the coating's effect on long-term barrier.

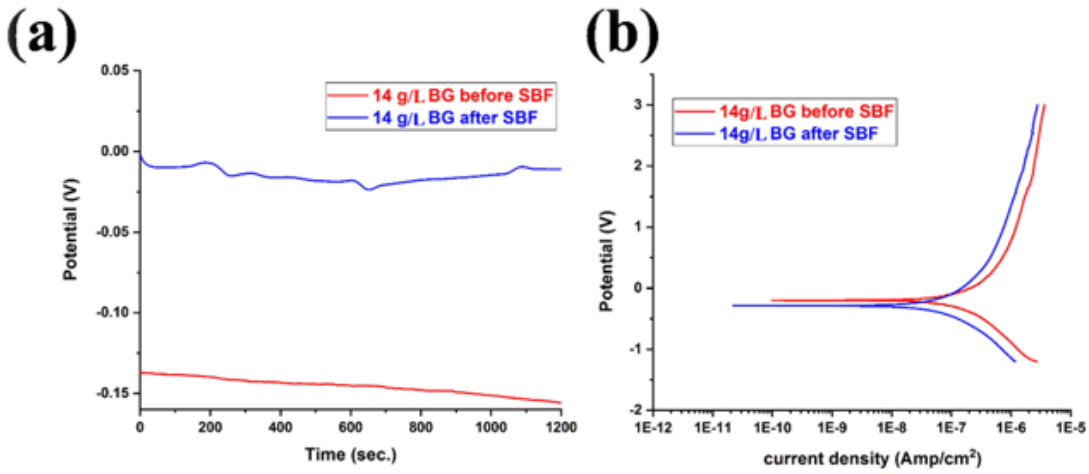

Fig. 13. (a) Open circuit potential (OCP) curves and (b) Tafel polarization plots of 14 g/L BG-coated Ti-6Al-7Nb substrate before and after one-month immersion in simulated body fluid (SBF)

Table 8. Corrosion parameters of 14 g/L BG-coated Ti-6Al-7Nb substrate after immersion in simulated body fluid (SBF)

ITEM	$E_{corr.}$ (volt)	$I_{corr.}$ (Amp.)	Corr. Rate (mmpy)	β_C	β_a	OCP (volt)
BG after SBF	-0.286	2.387×10^{-8}	2.073×10^{-4}	0.197	0.213	-0.011

3.13. XRD Analysis of Ti-6Al-7Nb coated with bioactive glass before and after immersion in simulated body fluid (SBF)

Fig. 14a shows the XRD patterns of the Ti-6Al-7Nb substrates pre-hydroxylated with bioactive glass (BG) with concentrations of 8, 11, and 14 g/L investigated before immersion inside simulated body fluids (SBF). The diffraction peaks were consistent with the crystalline structure of bioactive glass (Reference code: 01-082-1109) presented clear reflections at (301) (35.5°), (220) (38.2°), (221) (40.5°), (004) (53.0°), (150) (63.6°), (503) (70.8°), (324) (74.8°), (160) (76.7°), and (161) (78.1°) in the 2θ positions. The absence of titanium peaks indicates that the BG coating fully covered the substrate. With increasing BG concentration—most notably at 14 g/L—the peak intensity becomes sharper, suggesting better crystallinity and greater coating thickness. The phase purity is maintained, with no evidence of unwanted secondary phases. Fig. 14b presents the XRD profile of the coated sample after immersion in simulated body fluid (SBF). New peaks appeared indicating the formation of $Ca_{14.92}(PO_4)_{2.35}(SiO_4)_{5.65}$ and $CaSiO_3$, which are still consistent with Reference code: 01-082-1109. The apatite-silicate phase revealed reflections at (080) (32.9°), (160), (381) (46.1°), and (144) (57.3°) whereas calcium silicate $CaSiO_3$ appears at (220) (75.2°) and (224) (67.1°). The unique peak near 29° confirms apatite growth. The findings support the notion that the BG coating reacted with the surrounding fluid, allowing for the release of ions, consequently encouraging the formation of bioactive calcium phosphate-silicate layers. This transition indicates the coating's bioactivity and its ability to support apatite nucleation on the surface of the implant [47, 48].

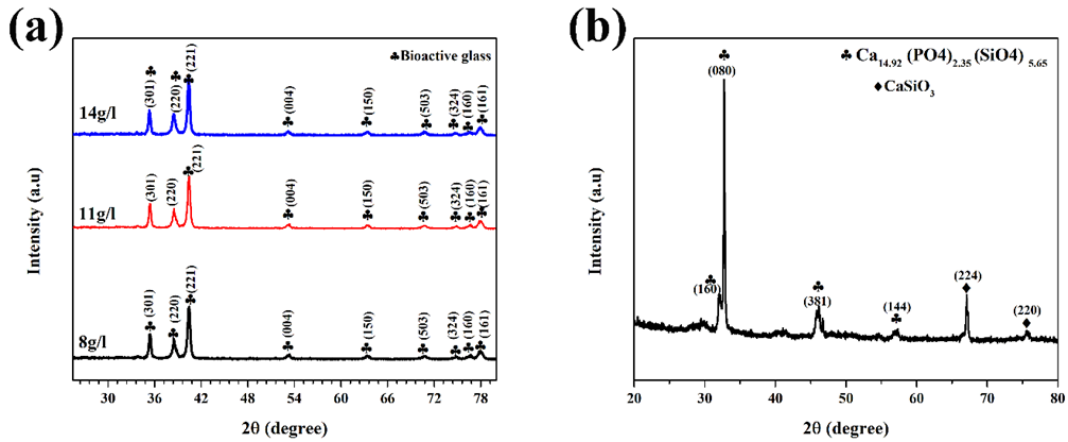

Fig. 14. XRD patterns of Ti-6Al-7Nb substrates coated with bioactive glass at different concentrations before (a) and after (b) immersion in SBF

3.14. Comparison with previous studies

Our results on HA/BG hybrid coatings show distinct performance trends when compared to published literature. In the study by Sola et al. (2019), HA/BG coatings prepared by EPD demonstrated corrosion rates in the range of 10^{-3} to 10^{-4} mmpy after SBF immersion. In contrast, our BG-rich coating (70% BG) achieved a significantly lower long-term corrosion rate of 9.096×10^{-5} mmpy, indicating superior passivation and surface sealing.

Similarly, Liu et al. (2021) reported zeta potential values between 10 and 15 mV for HA/BG suspensions, which were sufficient for moderate stability. In our work, the 14 g/L BG suspension achieved a zeta potential of 18.47 mV, reflecting better dispersion stability and improved coating uniformity.

Regarding antibacterial activity, previous studies such as Balasubramanian et al. (2020) reported inhibition zones of 18–22 mm for E. coli and S. aureus using BG-containing coatings. Our results showed inhibition zones up to 26 mm for E. coli and 23 mm for S. aureus, demonstrating stronger antibacterial efficacy, possibly due to the sustained ion release and synergistic effect between HA and BG phases.

The improved outcomes in our study can be attributed to optimized HA/BG ratios, controlled EPD parameters, and the use of triethanolamine (TEA) for enhanced particle dispersion, which together contributed to superior coating quality, bioactivity, and long-term corrosion resistance compared to existing reports.

4. Conclusion

- The SEM analysis of Ti-6Al-7Nb coated with varying bioactive glass (BG) concentrations reveals enhanced surface morphology with rising BG content. The uncoated substrate shows a smooth, particle-free surface. At 8 g/L BG, the coating is porous and uneven, while 11 g/L BG results in a more uniform and denser layer. The 14 g/L BG sample exhibits the most compact, continuous, and well-integrated coating, indicating it offers the most effective surface coverage and adhesion.
- The SEM analysis of Ti-6Al-7Nb substrates coated with bioactive glass (BG) at concentrations ranging from 8 to 14 g/L shows a steady improvement in surface morphology. The uncoated substrate (0 g/L) displays a smooth, particle-free surface. The coating at 8 g/L BG shows porous characteristics with uneven particle distribution and insufficient coverage. The coating becomes denser and more uniform when the BG concentration reaches 11 g/L while voids decrease. The highest concentration of 14 g/L BG produces a surface with a dense uniform structure that demonstrates the best coating effectiveness and adhesion.
- The thickness and uniformity of the coatings on Ti-6Al-7Nb substrates improved with increasing BG concentrations from 8 to 14 g/L. The coating thickness grew from 41.1 µm to 57.3 µm, and the thicker coatings became denser and more compact due to better particle availability and enhanced deposition efficiency.
- The electrochemical corrosion resistance of Ti-6Al-7Nb substrates rises as the bioactive glass concentration increases. The uncoated alloy shows a weak corrosion rate, while coatings with 8 g/L BG lower the corrosion current to 3.154×10^{-7} A and corrosion rate to 2.740×10^{-3} mmpy. Further enhancement is noted at 11 g/L BG (1.151×10^{-7} A, 1.000×10^{-3} mmpy), with the good protection achieved at 14 g/L BG, which shows the lowest corrosion current (5.190×10^{-8} A) and rate (4.509×10^{-4} mmpy). The increasingly positive open circuit potential confirms improved surface passivation and electrochemical stability with higher BG content.
- Ti-6Al-7Nb substrates with BG coatings displayed antibacterial performance through inhibition zones that measured 26 mm against E. coli and 23 mm against S. aureus thereby proving their ion-based antimicrobial properties. The coated surfaces maintained better bioactivity and protective properties than uncoated samples although they produced smaller inhibition zones.

Acknowledgment

The author gratefully acknowledges the support provided by the College of Engineering, University of Diyala, Baquba, Iraq. Sincere thanks are extended to the faculty members, laboratory staff, and all colleagues who contributed technical assistance and valuable discussions throughout the course of this research.

References

[1] O. Demontiero, C. Vidal, and G. Duque, "Aging and bone loss: New insights for the clinician," Ther. Adv. Musculoskelet. Dis., vol. 4, no. 2, pp. 61–76, 2012, doi: 10.1177/1759720X11430858.

[2] R. Drevet and H. Benhayoune, Biomaterials Design for Human Body Repair. Basel, Switzerland: MDPI, 2024.

[3] G. Li et al., "An overview of osteoporosis and frailty in the elderly," BMC Musculoskelet. Disord., vol. 18, Art. no. 46, 2017, doi: 10.1186/s12891-017-1411-3.

[4] K. Moghadasi et al., "A review on biomedical implant materials and the effect of friction stir based techniques on their mechanical and tribological properties," J. Mater. Res. Technol., vol. 17, pp. 1054–1121, 2022, doi: 10.1016/j.jmrt.2022.01.061.

[5] G. Renganathan, N. Tanneru, and S. L. Madurai, "Orthopedical and biomedical applications of titanium and zirconium metals," in Fundamental Biomaterials: Metals. Oxford, UK: Elsevier, 2018, pp. 211–241.

[6] S. Mutha, "Evolution and principles of metals and alloys used in orthopedic implantology," in Handbook of Orthopaedic Trauma Implantology. Cham, Switzerland: Springer, 2022, pp. 1–19.

[7] J. Zhou et al., "Evolution from bioinert to bioresorbable: In vivo comparative study of additively manufactured metal bone scaffolds," Adv. Sci., vol. 10, no. 26, Art. no. 2302702, 2023, doi: 10.1002/advs.202302702.

[8] R. M. Pilliar, "Metallic biomaterials," in Biomedical Materials. Boca Raton, FL, USA: CRC Press, 2009, pp. 41–81.

[9] K. Prasad et al., "Metallic biomaterials: Current challenges and opportunities," Materials, vol. 10, no. 8, Art. no. 884, 2017, doi: 10.3390/ma10080884.

[10] D. Zindani, K. Kumar, and J. P. Davim, "Metallic biomaterials—A review," in Mechanical Behaviour of Biomaterials. Sawston, UK: Woodhead Publishing, 2019, pp. 83–99.

[11] J. Huang, X. Li, and Z. Guo, "Biomechanical and biochemical compatibility in innovative biomaterials," in Biocompatibility and Performance of Medical Devices. Oxford, UK: Elsevier, 2020, pp. 23–46.

[12] M. A. Shayeb et al., "Bioactive surface modifications on dental implants: A systematic review and meta-analysis," Clin. Oral Investig., vol. 28, no. 11, Art. no. 592, 2024, doi: 10.1007/s00784-024-05892-1.

[13] G. Zhu, G. Wang, and J. J. Li, "Advances in implant surface modifications to improve osseointegration," Mater. Adv., vol. 2, no. 21, pp. 6901–6927, 2021, doi: 10.1039/D1MA00507A.

[14] Y. Liu et al., "Role of implant surface modification in osseointegration: A systematic review," J. Biomed. Mater. Res. A, vol. 108, no. 3, pp. 470–484, 2020, doi: 10.1002/jbm.a.36844.

[15] D. S. Brauer, "Bioactive glasses—Structure and properties," Angew. Chem. Int. Ed., vol. 54, no. 14, pp. 4160–4181, 2015, doi: 10.1002/anie.201405310.

[16] A. Hoppe, N. S. Güldal, and A. R. Boccaccini, "A review of the biological response to ionic dissolution products from bioactive glasses and glass-ceramics," Biomaterials, vol. 32, no. 11, pp. 2757–2774, 2011, doi: 10.1016/j.biomaterials.2011.01.004.

[17] P. A. Hassan, B. Balakrishnan, and A. K. Tyagi, Engineered Biomaterials: Progress and Prospects. Singapore: Springer, 2023.

[18] N. O. Joy-Anne et al., "Bioactive glass coatings on metallic implants for biomedical applications," Bioact. Mater., vol. 4, pp. 261–270, 2019, doi: 10.1016/j.bioactmat.2019.06.003.

[19] A. R. Boccaccini et al., "Polymer/bioactive glass nanocomposites for biomedical applications: A review," Compos. Sci. Technol., vol. 70, no. 13, pp. 1764–1776, 2010, doi: 10.1016/j.compscitech.2010.06.002.

[20] S. Albayrak and C. Gul, "Ceramic coatings for biomedical applications," in Fiber and Ceramic Filler-Based Polymer Composites for Biomedical Engineering. Cham, Switzerland: Springer, 2024, pp. 233–256.

[21] N. Nikam et al., "Advancements in surface coatings for enhancing longevity in hip implants: A review," Prosthesis, vol. 7, no. 1, Art. no. 21, 2025, doi: 10.3390/prosthesis7010021.

[22] H. Meskher et al., "Limitations, challenges and prospective solutions for bioactive glass-based nanocomposites for dental applications," J. Dent., Art. no. 105331, 2024, doi: 10.1016/j.jdent.2024.105331.

[23] A. Sola et al., "Bioactive glass coatings: A review," Surf. Eng., vol. 27, no. 8, pp. 560–572, 2011, doi: 10.1179/1743294411Y.0000000024.

[24] G. Brunello, H. Elsayed, and L. Biasetto, "Bioactive glass and silicate-based ceramic coatings on metallic implants," Materials, vol. 12, no. 18, Art. no. 2929, 2019, doi: 10.3390/ma12182929.

[25] R. Sergi, D. Bellucci, and V. Cannillo, "A comprehensive review of bioactive glass coatings," Coatings, vol. 10, no. 8, Art. no. 757, 2020, doi: 10.3390/coatings10080757.

[26] N. Eliaz and N. Metoki, "Calcium phosphate bioceramics," Materials, vol. 10, no. 4, Art. no. 334, 2017, doi: 10.3390/ma10040334.

[27] M. Maximov et al., "Bioactive glass—Preparation and coating methods," Coatings, vol. 11, no. 11, Art. no. 1386, 2021, doi: 10.3390/coatings11111386.

[28] R. Drevet, J. Fauré, and H. Benhayoune, "Electrophoretic deposition of bioactive glass coatings for bone implant applications," Coatings, vol. 14, no. 9, Art. no. 1084, 2024, doi: 10.3390/coatings14091084.

[29] N. I. Alyousef, A. T. Shahd, and A. S. Khana, "Bioactive glass coated dental implants," in Dental Implants: Materials, Coatings, Surface Modifications and Interfaces with Oral Tissues. Cambridge, UK: Woodhead Publishing, 2020, pp. 93–112.

[30] R. Drevet, J. Fauré, and H. Benhayoune, "Bioactive calcium phosphate coatings for bone implant applications," Coatings, vol. 13, no. 6, Art. no. 1091, 2023, doi: 10.3390/coatings13061091.

[31] A. R. Boccaccini et al., "Electrophoretic deposition of biomaterials," J. R. Soc. Interface, vol. 7, suppl. 5, pp. S581–S613, 2010, doi: 10.1098/rsif.2010.0156.focus.

[32] R. O. Hussein and D. O. Northwood, "Production of anti-corrosion coatings on light alloys by plasma electrolytic oxidation," in Developments in Corrosion Protection. London, UK: IntechOpen, 2014.

[33] R. Hussein, X. Nie, and D. Northwood, "Application of plasma electrolytic oxidation coatings on magnesium alloys," Corros. Mater., vol. 38, no. 1, pp. 55–65, 2013.

[34] A. Thakur et al., "Recent advancements in surface modification for enhancing biocompatibility," Coatings, vol. 12, no. 10, Art. no. 1459, 2022, doi: 10.3390/coatings12101459.

[35] S. Singh, G. Singh, and N. Bala, "Electrophoretic deposition of bioactive glass composite coatings," Mater. Today Proc., vol. 5, no. 9, pp. 20160–20169, 2018, doi: 10.1016/j.matpr.2018.06.385.

[36] H. Zhang et al., "Characteristics of marine biomaterials and their applications," Mar. Drugs, vol. 20, no. 6, Art. no. 372, 2022, doi: 10.3390/md20060372.
[37] S. Karmakar et al., "Nanoparticle deposition techniques for silica nanoparticles," arXiv:2503.22593, 2025.
[38] D. Zhang et al., "Electrophoretic deposition of high adhesion energetic coatings," Chem. Eng. J., vol. 511, Art. no. 162187, 2025, doi: 10.1016/j.cej.2024.162187.
[39] M. K. Hassan et al., "Enhancement of adhesion strength and in vivo evaluation of electrodeposited calcium phosphate/chitosan coatings," Surf. Interfaces, vol. 42, Art. no. 103475, 2023, doi: 10.1016/j.surfin.2023.103475.
[40] R. Souza et al., "Surface finishing and shape effects on corrosion resistance of Ti–6Al–4V," Mater. Res., vol. 25, Art. no. e20210546, 2022, doi: 10.1590/1980-5373-mr-2021-0546.
[41] J. Barajas et al., "Influence of process parameters on electrophoretic deposition of zirconia nanoparticle coatings," in J. Phys.: Conf. Ser., vol. 985, Art. no. 012018, 2018, doi: 10.1088/1742-6596/985/1/012018.
[42] A. Doostmohammadi et al., "Bioactive glass nanoparticles with negative zeta potential," Ceram. Int., vol. 37, no. 7, pp. 2311–2316, 2011, doi: 10.1016/j.ceramint.2011.05.046.
[43] F. Baino, "Quantifying the adhesion of silicate glass–ceramic coatings," Materials, vol. 12, no. 11, Art. no. 1754, 2019, doi: 10.3390/ma12111754.
[44] S. Khanmohammadi, M. O. Ilkhchi, and J. Khalil-Allafi, "Electrophoretic deposition of bioglass–whisker hydroxyapatite coatings," Surf. Coat. Technol., vol. 378, Art. no. 124949, 2019, doi: 10.1016/j.surfcoat.2019.124949.
[45] S. Ferraris et al., "Zeta potential measurements on solid surfaces for in vitro biomaterials testing," Front. Bioeng. Biotechnol., vol. 6, Art. no. 60, 2018, doi: 10.3389/fbioe.2018.00060.
[46] A.-P. Forsback et al., "Effect of ionic variables on biomimetic mineralization," Key Eng. Mater., vol. 240, pp. 249–252, 2002, doi: 10.4028/www.scientific.net/KEM.240.249.
[47] C. Liu, C.-W. Chen, and P. Ducheyne, "In vitro surface reaction layer formation of calcium phosphate cement–bioactive glass composites," Biomed. Mater., vol. 3, no. 3, Art. no. 034111, 2008, doi: 10.1088/1748-6041/3/3/034111.
[48] R. Narayanan et al., "Calcium phosphate-based coatings on titanium and its alloys," J. Biomed. Mater. Res. B, vol. 85, no. 1, pp. 279–299, 2008, doi: 10.1002/jbm.b.30932.